IEEE Access
Multidisciplinary | Rapid Review | Open Access Journal

Received January 3, 2019, accepted February 6, 2019, date of publication February 12, 2019, date of current version March 5, 2019.

Digital Object Identifier 10.1109/ACCESS.2019.2898687

Grid Voltage Sensorless Model-Based Predictive Power Control of PWM Rectifiers Based on Sliding Mode Virtual Flux Observer

JIEJUNYI LIANG[1], HAIQING WANG[2], AND ZHENGFENG YAN[3]

[1]School of Automotive Engineering, Wuhan University of Technology, Wuhan 430070, China
[2]Faculty of Engineering and Information Technology, University of Technology Sydney, Ultimo, NSW 2007, Australia
[3]School of Automotive and Transportation Engineering, Hefei University of Technology, Hefei 230009, China

Corresponding author: Haiqing Wang (zoey.hq.wang@gmail.com)

This work was supported by the State Scholarship Fund of China Scholarship Council under Grant 201706695018.

ABSTRACT In this paper, a grid voltage sensorless model predictive control is proposed based on a sliding mode virtual flux observer (SMVFO). The proposed SMVFO shows good inherent filtering capacity, and thus there is no high-frequency chattering problem. In addition, the proposed SMVFO is designed based on the closed-loop current estimation. Not only is DC-drift issue solved but also dynamic response is enhanced when compared with the prior open-loop virtual flux observer. To verify the effectiveness of the presented SMVFO, it is further integrated into finite control set-model predictive control (FCS-MPC) for pulse width modulator (PWM) rectifiers. The whole control algorithm features simplicity and improved cost-effectiveness due to the absence of modulator and grid voltage sensors. As the SMVFO can predict current at the next sampling instant while estimating virtual flux accurately, the proposed SMVFO assisted FCS-MPC is comparable to its counterpart using measured grid voltage. The simulation and experimental tests were carried out on a two-level voltage source PWM rectifier to validate the effectiveness of the proposed method.

INDEX TERMS Predictive power control, voltage sensorless, sliding mode observer, PWM rectifier.

I. INTRODUCTION

Due to the desirable capability of dealing with the nonlinear control problems, model predictive control (MPC) has attracted the attentions of researchers from the academic world as a promising control strategy for power converter and electric drive control schemes [1], [2]. Although the product-level implementations of this approach in the industries are still constrained, the development of powerful processors makes it possible for wide applications for power converters and electric drives [3], [4].

In the context of power converter applications, there are generally two types of MPC which are the continuous control set MPC (CCS-MPC) [5] and the finite control set MPC according to the inclusion of continuous reference voltage vector and the necessity of pulse width modulator [6], [7]. The virtues of MPC include the fast dynamics performance, the simple structure and the easy implementations, especially for FSC-MPC due to its intuitive modeling and the straightforward handing of constrains [8].

The associate editor coordinating the review of this manuscript and approving it for publication was Fengjiang Wu.

However, FCS-MPC also has its own limitations. Although many researches have been done in order to improve the performance of FCS-MPC [9]–[12], the limitation such as the computational cost, the parameter tuning and the sensorless operation still need to be further investigated and the corresponding solutions are imperative [13]–[15].

Generally, there are two well investigated approaches which are the direct power control (DPC) method [16]–[18] and the voltage-oriented control (VOC) method [19], [20] for the control of voltage source rectifier (VSR). For VOC, in order to get desirable performance, adequate tuning work should be done as it is based on the synchronously rotating frame and usually adopts two proportional-integral (PI) controllers to regulate the current. DPC was then proposed as an alternative for VOC. Other than current control loops, power controllers are employed in DPC and before the implementation, predefined selecting rules or lookup tables should be constructed according to the instantaneous power characters. Based on the differences between the measured and the reference values of the active and reactive powers, and grid voltage or the estimated virtual flux vector [21], the optimal switching state could be then decided. DPC owns the merits of fast

dynamic performance and at the same time keeps simple and robust. However, it still suffers from high power ripples and current distortion. To obtain a desirable performance, a relatively high sampling frequency is often necessary for DPC.

On the contrast, FCS-MPC is more flexible when dealing with constraints and could achieve better overall performance when handling systems with conflicting control objectives like the conflicts between the performance in steady-state and the low switching frequency operation.

In order to accurately control the active and reactive power, the grid voltage information is essential. However, in order to acquire the voltage information, expensive voltage sensor is necessary which also requires additional mounting space. These two factors present considerable challenges when conducting large scale implementations. As a result, voltage sensorless based schemes have been the focus of recent researches [22]–[24]. There are many virtues of the sensorless schemes such as the reliability, the relatively low implementing cost, and the reduced volume following the less wire connections and the corresponding machinery installation. Moreover, as continuous operation is of great importance in the control, the sensorless methods could be adopted as a complementary strategy when the sensors encounter some fatal faults. In order to further improve the control performance, virtual flux (VF) based strategy is brought out in [25], where the estimated VF and the actual grid currents could be used to calculate the powers, leading to many advantages which include the low sampling frequency, lower current total harmonic distortion and the easy estimations of powers and voltages.

There are many successful implementations of VF estimator. With VF, it becomes possible for VOC, DPC and FCS-MPC to be implemented without measuring the grid voltage. In prior research, most VF estimators are developed based on the principle of integrating grid voltage. However, in the real time implementations, the pure open-loop integrator would still compromise the overall performance due to the dc-drift problem. VF was adopted to obtain the main voltage from the switching state, line currents and dc voltage in [26] to construct a decoupling hysteresis current controller (DHC). In [27], a VF based Predictive direct power control (P-DPC) was proposed. Conventionally, the measured grid voltages and currents were used to calculate the instantaneous powers with the drawbacks of high sampling frequency and choke inductance, and the dependence on the switching state. In the proposed method, VF was adopted to eliminate the use of ac-side voltage sensors. In [28], a VF based DPC control strategy was developed where the VF vector was computed using the grid voltage vector and was used to obtain the instantaneous power. A first-order low pass filter was adopted to overcome the dc-drift problem associated with pure integrators. However, this method still cannot perfectly solve the problem by adopting low pass filters or band-pass filters as there would be a long settling time in transient processes or in the case of power-on due to the filters' slow converging rate.

In order to solve the aforementioned problem, achieving fast dynamic response and better robustness against external disturbances, the closed-loop observer stands out due to the feedback of the current estimation error when compared with open loop VF estimator. As a result, in order to track the virtual flux, a sliding mode observer (SMO) is designed in this paper based on closed-loop current estimation. SMO as an observer estimation method has been widely adopted in sensorless control strategy due to the virtues of robustness, nonlinearity, desirable dynamic performance and the high observation accuracy [29]. However, it still suffers from the high-frequency chattering problem because of the discontinuity of the sliding mode variable structure [30]. Moreover, the absence of modulator in the application of FCS-MPC will result in discreteness of the input converter voltage, which would further introduce switching harmonics in the grid voltage estimation. In order to cope with the switching harmonics and the ripples, a low pass filter could be adopted to generate a smooth estimation [31]. However, the accuracy of the voltage magnitude and the phase angle would be inevitably deteriorated, resulting in deviations of the actual power from its reference. Similarly, a sliding-mode virtual flux observer, which estimates the grid voltage first and then calculate virtual flux by integrating the estimated grid voltage, was proposed in [32]. To suppress the high-frequency chattering in the estimated grid voltage, sigmoid function is applied instead of sign function. Additionally, to solve the dc-drift problem of pure integral, a low pass filter with dynamic compensation scheme was applied. By comparison, the proposed method directly gives the estimation of virtual flux, which is simpler in concept and algorithm implementation. Moreover, there is no requirement of additional filter in the proposed observer due to inherent filtering capacity.

In this paper, the virtual flux is estimated by the developed SMO which is constructed based on the system model and the measured current. It is shown that once the sliding mode surface is arrived, the fundamental components of virtual flux can be accurately extracted by the proposed sliding-mode virtual flux observer. Theoretical analysis show that the estimated virtual flux is its actual value and disturbance passing an inherent complex-coefficient filter. Hence, there is no high-frequency chattering or DC drift problem in the developed SMVFO. Simulation and experimental tests confirm that the SMVFO based grid-voltage sensorless FCS-MPC is comparable with the conventional voltage sensor-based FCS-MPC.

The organization of this paper is as follows. The model construction of VSR is described in Section II. In Section III, the basic principles of the proposed SMVFO is presented followed by corresponding analysis. Section IV introduce the mathematical model of FCS-MPC and its implementation based on the proposed SMVFO. The simulation and experimental results and analysis are presented in Section V. Conclusions are drawn in Section VI.

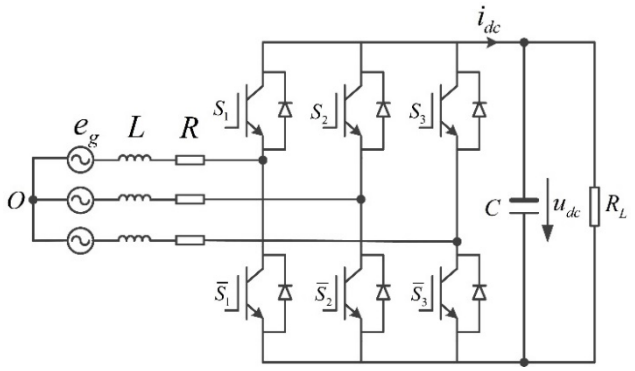

FIGURE 1. The diagram of the two-level PWM rectifier.

II. MATHEMATICAL MODEL OF PWM RECTIFIER

A schematic configuration of a two-level PWM rectifier is shown in Figure 1.

The mathematical model of the PWM rectifier in $\alpha\beta$ stationary reference can be described using the following equation:

$$L\begin{pmatrix}\frac{di_{g\alpha}}{dt}\\ \frac{di_{g\beta}}{dt}\end{pmatrix}=\begin{pmatrix}e_{g\alpha}\\ e_{g\beta}\end{pmatrix}-R\begin{pmatrix}i_{g\alpha}\\ i_{g\beta}\end{pmatrix}-\begin{pmatrix}u_{c\alpha}\\ u_{c\beta}\end{pmatrix} \tag{1}$$

where L is the filter inductance, R is the equivalent resistance of the filter, $i_{g\alpha}$ and $i_{g\beta}$ are the grid currents, $e_{g\alpha}$ and $i_{g\beta}$ are the grid voltage, $u_{c\alpha}$ and $u_{c\beta}$ are the converter voltage.

For the concept of VF, it can be computed as the integral of the voltage e, and then the definition of the flux ψ is expressed as

$$\psi_{\alpha\beta}=\int e_{\alpha\beta}\cdot dt=\begin{pmatrix}\psi_\alpha\\ \psi_\beta\end{pmatrix}=\begin{pmatrix}\int e_{g\alpha}\cdot dt\\ \int e_{g\beta}\cdot dt\end{pmatrix} \tag{2}$$

The grid voltage space vector can be then calculated as

$$\begin{pmatrix}e_{g\alpha}\\ e_{g\beta}\end{pmatrix}=\begin{pmatrix}\frac{d\psi_\alpha}{dt}\\ \frac{d\psi_\beta}{dt}\end{pmatrix}=\begin{pmatrix}d_\alpha-\omega\psi_\beta\\ d_\beta+\omega\psi_\alpha\end{pmatrix} \tag{3}$$

where d_α and d_β are the unknown disturbances including the magnitude variation and the harmonics, ω is the grid voltage frequency.

Substitute (3) into (2), the following equation can be obtained:

$$L\begin{pmatrix}\frac{di_{g\alpha}}{dt}\\ \frac{di_{g\beta}}{dt}\end{pmatrix}=\begin{pmatrix}-\omega\psi_\beta\\ \omega\psi_\alpha\end{pmatrix}-R\begin{pmatrix}i_{g\alpha}\\ i_{g\beta}\end{pmatrix}-\begin{pmatrix}u_{c\alpha}\\ u_{c\beta}\end{pmatrix}+\begin{pmatrix}d_\alpha\\ d_\beta\end{pmatrix} \tag{4}$$

As the forward Euler discretization has the merits of simplicity and acceptable accuracy [33] with a relatively short sampling period T_{sc}, it is adopted here to predict the current, neglecting the unknown disturbances, using the following expression

$$\begin{pmatrix}i_{g\alpha}^{k+1}\\ i_{g\beta}^{k+1}\end{pmatrix}=\begin{pmatrix}i_{g\alpha}^{k}\\ i_{g\beta}^{k}\end{pmatrix}+\frac{T_{sc}}{L}\begin{pmatrix}e_{g\alpha}^{k}\\ e_{g\beta}^{k}\end{pmatrix}-\frac{T_{sc}}{L}\begin{pmatrix}Ri_{g\alpha}^{k}\\ Ri_{g\beta}^{k}\end{pmatrix}-\frac{T_{sc}}{L}\begin{pmatrix}u_{c\alpha}^{k}\\ u_{c\beta}^{k}\end{pmatrix} \tag{5}$$

where the superscript k is for the variable at the kth instant.

Additionally, the active and reactive power p and q can be calculate as

$$\begin{aligned}P&=\mathrm{Re}(\boldsymbol{e}\cdot\boldsymbol{i}^*)\\ Q&=\mathrm{Im}(\boldsymbol{e}\cdot\boldsymbol{i}^*)\end{aligned} \tag{6}$$

where $\boldsymbol{e}=e_{g\alpha}+je_{g\beta}$ is the grid voltage vector, $\boldsymbol{i}=i_{g\alpha}+ji_{g\beta}$ is the grid current vector, and the superscript $*$ represents the conjugation of a complex variable.

Using (6), a more detailed expression for P and Q can be derived (7)

$$P+jQ=\left\{\left(d_\alpha-\omega\psi_\beta\right)+j\left(d_\beta+\omega\psi_\alpha\right)\right\}\left(i_{ga}+ji_{g\beta}\right)^* \tag{7}$$

Omitting the unknown disturbances, the active and reactive powers can be calculated as follows

$$P=\left\{\omega\left(\psi_\alpha i_{g\beta}-\psi_\beta i_{g\alpha}\right)\right\} \tag{8}$$

$$Q=\left\{\omega\left(\psi_\alpha i_{g\alpha}+\psi_\beta i_{g\beta}\right)\right\} \tag{9}$$

III. SLIDING-MODE VIRTUAL FLUX OBSERVER

A. CONSTRUCTION OF THE PROPOSED SMVFO

In order to estimate the grid voltage, a SMVFO is designed based on (3) and (4) as follows.

$$L\begin{pmatrix}\frac{d\hat{i}_{g\alpha}}{dt}\\ \frac{d\hat{i}_{g\beta}}{dt}\end{pmatrix}=\begin{pmatrix}-\omega\hat{\psi}_\beta+u_{\alpha smo}\\ \omega\hat{\psi}_\alpha+u_{\beta smo}\end{pmatrix}-R\begin{pmatrix}\hat{i}_{g\alpha}\\ \hat{i}_{g\beta}\end{pmatrix}-\begin{pmatrix}u_{c\alpha}\\ u_{c\beta}\end{pmatrix} \tag{10}$$

$$\begin{pmatrix}\frac{d\hat{\psi}_\alpha}{dt}\\ \frac{d\hat{\psi}_\beta}{dt}\end{pmatrix}=\begin{pmatrix}-\omega\hat{\psi}_\beta-m\cdot u_{\beta smo}\\ \omega\hat{\psi}_\alpha+m\cdot u_{\alpha smo}\end{pmatrix} \tag{11}$$

where m represent the parameter of the sliding mode observer, the hat "$\hat{\ }$" is for the estimated variables, $\boldsymbol{u}_{smo}$ is the control function. Using (3), (4), (10) and (11), the error equations can be obtained as

$$L\begin{pmatrix}\frac{df_{i\alpha}}{dt}\\ \frac{df_{i\beta}}{dt}\end{pmatrix}=\begin{pmatrix}-\omega f_{\psi\beta}\\ \omega f_{\psi\alpha}\end{pmatrix}-\begin{pmatrix}u_{\alpha smo}\\ u_{\beta smo}\end{pmatrix}-R\begin{pmatrix}f_{i\alpha}\\ f_{i\beta}\end{pmatrix}+\begin{pmatrix}d_\alpha\\ d_\beta\end{pmatrix} \tag{12}$$

$$\begin{pmatrix} \frac{df_{\psi\alpha}}{dt} \\ \frac{df_{\psi\beta}}{dt} \end{pmatrix} = \begin{pmatrix} d_\alpha - \omega f_{\psi\beta} + m \cdot u_{\beta smo} \\ d_\beta + \omega f_{\psi\alpha} - m \cdot u_{\alpha smo} \end{pmatrix} \tag{13}$$

where $f_{i\alpha} = i_{g\alpha} - \hat{i}_{g\alpha}$, $f_{i\beta} = i_{g\beta} - \hat{i}_{g\beta}$ are the current estimation errors, $f_{\psi\beta} = (\psi_\beta - \hat{\psi}_\beta)$ and $f_{\psi\alpha} = (\psi_\alpha - \hat{\psi}_\alpha)$ are the virtual flux estimation errors.

Moreover, the linear sliding-mode surface is employed, and the expression is shown below.

$$\begin{aligned} z_\alpha &= i_{ga} - \hat{i}_{ga} \\ z_\beta &= i_{g\beta} - \hat{i}_{g\beta} \end{aligned} \tag{14}$$

The exponential reaching law is adopted in order to develop the sliding-mode control function and the expression is

$$\frac{dz}{dt} = -\lambda sgn(z) - \sigma z \tag{15}$$

where λ and σ are the reaching law parameters and the value of them are always greater than zero. The duration for the state variable starting from the initial z_0 to arrive $z(t) = 0$ can be calculated by

$$t = \frac{\ln(\lambda + \sigma |z_0|) - \ln \lambda}{\sigma} \tag{16}$$

To illustrate the influence of λ and σ on the converging time, the relationship is shown in Figure 2. It could can be seen that the larger λ and σ are, the shorter the converging time is. However, the chattering level will also be higher with the rise of λ and σ, as well as the vulnerability of the system against the measurement noises.

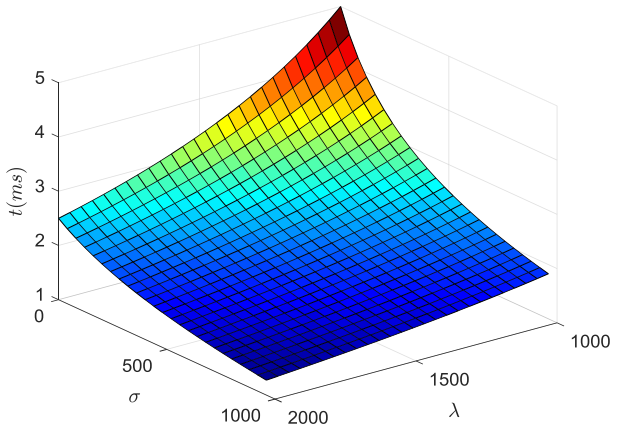

FIGURE 2. Converging time with varying λ and σ.

The equations below can be obtained according to (12)-(15)

$$\begin{pmatrix} -L\lambda sgn(f_{i\alpha}) - L\sigma f_{i\alpha} \\ -L\lambda sgn(f_{i\beta}) - L\sigma f_{i\beta} \end{pmatrix} = \begin{pmatrix} -\omega f_{\psi\beta} \\ \omega f_{\psi\alpha} \end{pmatrix} - \begin{pmatrix} u_{\alpha smo} \\ u_{\beta smo} \end{pmatrix} - R\begin{pmatrix} f_{i\alpha} \\ f_{i\beta} \end{pmatrix} + \begin{pmatrix} d_\alpha \\ d_\beta \end{pmatrix} \tag{17}$$

As $f_{\psi\alpha}$, $f_{\psi\beta}$, d_α and d_β are unknown disturbances, the control function u_{smo} can be designed as

$$\begin{pmatrix} u_{\alpha smo} \\ u_{\beta smo} \end{pmatrix} = \begin{pmatrix} L\lambda sgn(f_{i\alpha}) + (L\sigma - R) f_{i\alpha} \\ L\lambda sgn(f_{i\beta}) + (L\sigma - R) f_{i\beta} \end{pmatrix} \tag{18}$$

B. INVESTIGATION OF THE DESIGNED SMVFO

In order to verify the stability of the proposed SMVFO, the following defined Lyapunov function should be satisfied:

$$\begin{aligned} \dot{F}_\alpha &= z_\alpha \cdot \dot{z}_\alpha \le 0 \\ \dot{F}_\beta &= z_\beta \cdot \dot{z}_\beta \le 0 \end{aligned} \tag{19}$$

To calculate the Lyapunov function, (12), (13) and (18) should be referred and the expression is

$$\begin{aligned} \dot{V}_\alpha &= \frac{(d_\alpha - \omega f_{\psi\beta}) \cdot f_{i\alpha}}{L} - \lambda sgn(f_{i\alpha}) f_{i\alpha} - \sigma f_{i\alpha}^2 \\ &= \begin{cases} -\left(\sigma f_{i\alpha}^2 + (\lambda - \frac{(d_\alpha - \omega f_{\psi\beta})}{L}) |f_{i\alpha}|\right) & f_{i\alpha} \ge 0 \\ -\left(\sigma f_{i\alpha}^2 + (\lambda + \frac{(d_\alpha - \omega f_{\psi\beta})}{L}) |f_{i\alpha}|\right) & f_{i\alpha} < 0 \end{cases} \end{aligned} \tag{20}$$

In order to satisfy $\dot{V}_\alpha \le 0$, the constrain for λ is shown as

$$\lambda > \frac{|d_\alpha - \omega f_{\psi\beta}|}{L} \tag{21}$$

For $\dot{V}_\beta \le 0$, λ should satisfy the following equation neglecting the tedious derivation:

$$\lambda > \frac{|d_\beta + \omega f_{\psi\alpha}|}{L} \tag{22}$$

To ensure the SMVFO could reach the sliding-mode surface in a finite duration and stay on it, λ should satisfy the following constrains

$$\lambda > \frac{\max\left(|d_\alpha - \omega f_{\psi\beta}|, |d_\beta + \omega f_{\psi\alpha}|\right)}{L} \tag{23}$$

The current errors $f_{i\alpha}$, $f_{i\beta}$ and the corresponding derivatives will converge to zero when the sliding-mode surface is reached. According to (12) and (13), the control function could be obtained as:

$$\begin{aligned} u_{\alpha smo} &= d_\alpha - \omega f_{\psi\beta} \\ u_{\beta smo} &= d_\beta + \omega f_{\psi\alpha} \end{aligned} \tag{24}$$

According to (11), the control function can be further expressed as

$$\begin{aligned} u_{\alpha smo} &= \frac{1}{m}\left(\frac{d\hat{\psi}_\beta}{dt} - \omega\hat{\psi}_\alpha\right) \\ u_{\beta smo} &= \frac{1}{m}\left(-\frac{d\hat{\psi}_\alpha}{dt} - \omega\hat{\psi}_\beta\right) \end{aligned} \tag{25}$$

The relationship between the estimated VF and the actual value in complex vector form can be then obtained and shown below

$$\hat{\boldsymbol{\psi}} = \frac{m\boldsymbol{\psi} + m\boldsymbol{d}}{s - j\omega + m} \tag{26}$$

One can see that the estimated virtual flux is the result of its actual value and unknown disturbances passing the following complex coefficient filter.

$$F(s) = \frac{m}{s - j\omega + m} \tag{27}$$

The magnitude-frequency characteristic of $F(s)$ is demonstrated in Figure 3.

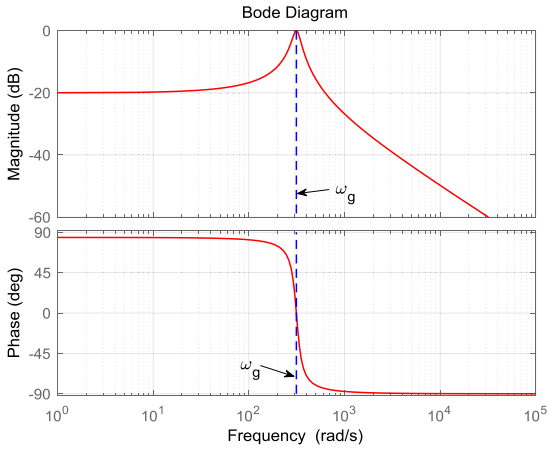

FIGURE 3. Bode plot of $F(s)$ in (28).

It can be seen that the fundament component of the virtual flux can be desirably tracked by the estimated virtual flux without phase and magnitude error and could also be validated by (eq27) where $F(j\omega) = 1$. Moreover, as the main reasons for the disturbance are the harmonics and the dc-bias, it could be coped well with a properly chosen m. The influence m can be also revealed in Figure 3. For a better distrubances rejection performance, a smaller m should be chosen, however, the converging rate will be compromised. On the contrary, in order to have a faster converging rate, a higher m shold be chosen, and correspondingly, the ability to reject disturbances will be worse. As a result, a proper m should be determined according to the need of the steady state performance and the dynamic performance.

C. DISCRETE-TIME IMPLEMENTATION OF SMVFO

In order to have digital implementations, the proposed SMVFO should be discretized first. Forward Euler discretization approach is adopted here as the adopted sampling frequency is small enough where $T_{sc} = 50\mu s$. Generally, if the ratio of the sampling frequency f_s over the frequency of the concerned state variable f_e, i.e. $F_{ratio} = f_s/f_e$, is sufficiently high ($F_{ratio} > 30$), the accuracy of the forward Euler discretization is usually satisfactory [34]. In this study, $F_{ratio} = 2*\frac{10^4}{50} = 400$ which is sufficiently high to guarantee the accuracy. The discretized SMVFO equations are shown below.

$$\begin{pmatrix} u^k_{\alpha smo} \\ u^k_{\beta smo} \end{pmatrix} = \begin{pmatrix} L\lambda \mathrm{sgn}(f^k_{i\alpha}) + (L\sigma - R) f^k_{i\alpha} \\ L\lambda \mathrm{sgn}(f^k_{i\beta}) + (L\sigma - R) f^k_{i\beta} \end{pmatrix} \tag{28}$$

$$\begin{pmatrix} \hat{\psi}^{k+1}_\alpha \\ \hat{\psi}^{k+1}_\beta \end{pmatrix} = \begin{pmatrix} \hat{\psi}^k_\alpha \\ \hat{\psi}^k_\beta \end{pmatrix} + T_{sc} \begin{pmatrix} -\omega\hat{\psi}^k_\beta - m \cdot u^k_{\beta smo} \\ \omega\hat{\psi}^k_\alpha + m \cdot u^k_{\alpha smo} \end{pmatrix} \tag{29}$$

$$\begin{pmatrix} \hat{i}^{k+1}_{g\alpha} \\ \hat{i}^{k+1}_{g\beta} \end{pmatrix} = \begin{pmatrix} \hat{i}^k_{g\alpha} \\ \hat{i}^k_{g\beta} \end{pmatrix} + \frac{T_{sc}}{L} \begin{pmatrix} -\omega\hat{\psi}^k_\beta + u^k_{\alpha smo} - u^k_{c\alpha} - R\hat{i}^k_{g\alpha} \\ \omega\hat{\psi}^k_\alpha + u^k_{\beta smo} - u^k_{c\beta} - R\hat{i}^k_{g\beta} \end{pmatrix} \tag{30}$$

IV. CONSTRUCTION OF FCS-MPC

Figure 4 shows the schematic flow chart of the proposed control method. It reveals the merit of the proposed method that only the grid current is needed to be measured. The outer control loop is neglected here as the main focus of this paper is to discuss the power control.

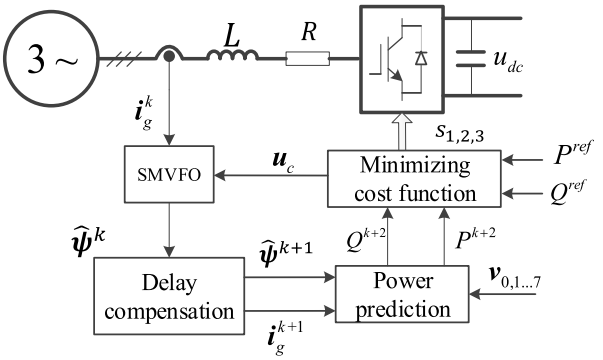

FIGURE 4. Block diagram of the SMVFO based FCS-MPC.

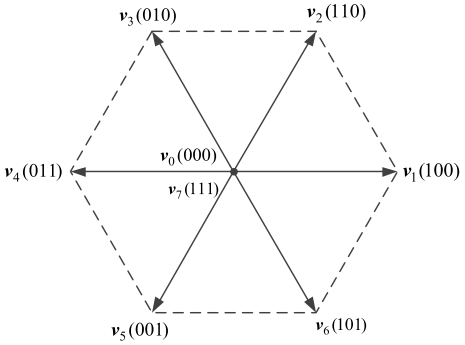

FIGURE 5. Illustration of switching states and voltage vectors of a two-level PWM rectifier.

There are 7 different voltage vectors and 8 switching states $v_{0,1...7}$ where v_0 and v_7 are the same voltage vector for a two-level VSR. The switching states and the voltage vectors are shown in Figure 5.

In implementations, there would be a lag between the actual voltage and the reference voltage as the sampling and the processing would take some time. In order to investigate how each voltage vector would affect the power tracking performance, the selected voltage vector should firstly be applied from $(k+1)$th instant to $(k+2)$th instant, and then predict the active and reactive power at $(k+2)$th instant.

In order to predict the grid current $i^{k+2}_{gi} (i = 0, 1 \ldots 7)$ using (5) for $v_{0,1...7}$ at the $(k+2)$th instant, the voltage vector selected during the previous control period should be used to

predict $\boldsymbol{i}_g^{k+1}$. The complex power can then be expressed as the following equations after obtaining $\boldsymbol{i}_{gi}^{k+2}$.

$$\boldsymbol{S}_i^{k+2} = 1.5\left(\boldsymbol{i}_{gi}^{k+2}\right)^* \odot \left(\hat{\boldsymbol{\psi}}^k e^{j2\omega T_{sc}}\right) \tag{31}$$

To compensate for the digital delay, the phase angle of the virtual flux is added by two control periods in (31). The cost function could be obtained which is shown below after getting S_i^{k+2}.

$$G_i = \left|S^{ref} - S_i^{k+2}\right| \tag{32}$$

The most desirable voltage vector $\boldsymbol{u}_{op}$ will be selected among the voltage vectors $\boldsymbol{v}_{0,1\ldots7}$ of a two-level PWM rectifier shown in Figure 5 by minimizing the cost function (32). The voltage vectors $\boldsymbol{v}_{0,1\ldots7}$ are calculated according to their switching states and the measured DC-link voltage u_{dc}, e.g., $\boldsymbol{v}_2$ is calculated as

$$v_2 = \frac{2}{3}u_{dc}\left(1 + e^{j2\pi/3} + 0 * e^{j4\pi/3}\right) = \frac{1}{3}u_{dc}\left(1 + j\sqrt{3}\right) \tag{33}$$

After the optimal voltage vector $\boldsymbol{u}_{op}$ is selected, the corresponding switching states are updated for the PWM rectifier so that the selected voltage vector will be output in the next sampling instant. Figure 6 shows the proposed integrated approach.

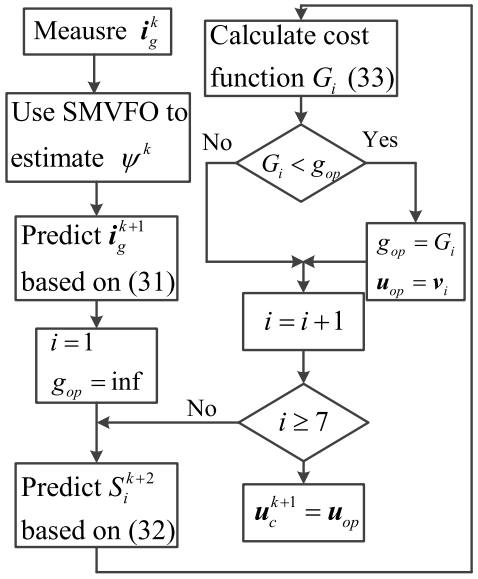

FIGURE 6. Flow chart of the proposed SMVFO based FCS-MPC.

V. SIMULATION AND EXPERIMENT ANALYSIS

The simulation and experiment for both the steady state and dynamic performance of the proposed method are conducted to demonstrate its effectiveness. Table 1 shows the main parameters. In all the presented results, the estimated power $\hat{P}$ and $\hat{Q}$ are calculated using (eq8) and (eq9) based on the estimated virtual flux while the actual power P and Q are computed using (eq6) based on the actual grid voltage and current.

TABLE 1. System parameters.

SYSTEM PARAMETERS	SYMBOL	VALUE
Line resistance	R	0.28Ω
Line inductance	L	10.5mH
Line-line voltage	e_N	150V
Line voltage frequency	ω	$2\pi * 50$ rad/s
Load resistance	R_L	101Ω
Sampling period	T_{sc}	50μs

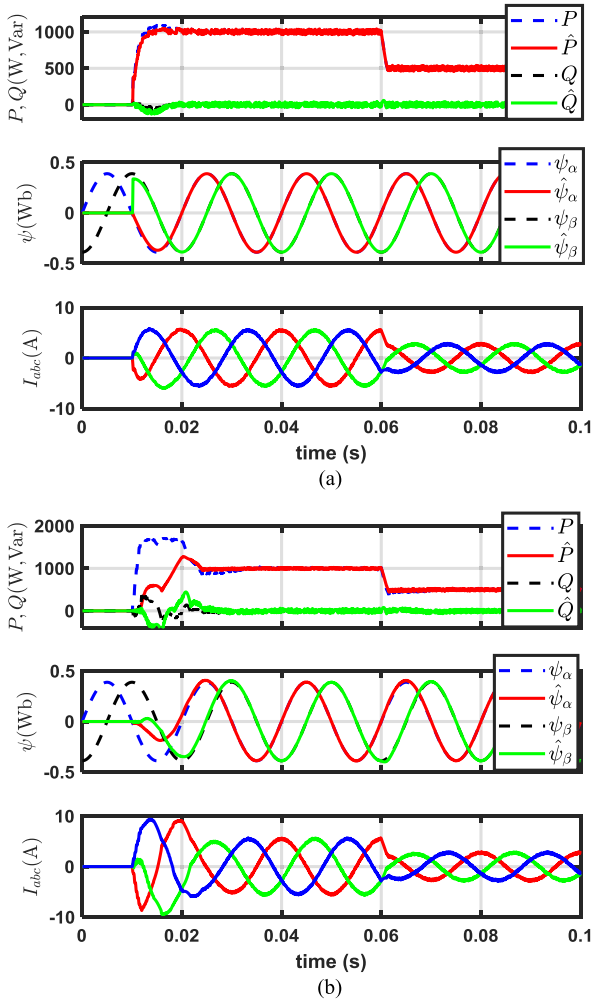

FIGURE 7. Simulated responses of startup response. (a) Response of SMVFO based FCS_MPC. (b) Response of prior virtual-flux observer [28] based FCS_MPC.

A. SIMULATION ANALYSIS

The simulation performance of the proposed SMVFO and the prior virtual-flux observer [28] based FCS-MPC during a startup process with the rated power reference are shown in Figure 7. The power and current waveforms are shown in the first and the third figure of Figure 7 (a), respectively, where no large overshoots and spikes occurred, proving the converging performance of the proposed method. To further demonstrate the fast converging ability of the method, the grid voltages are shown in the middle figure of Figure 7 (a)

where the estimated virtual flux $\hat{\psi}_\alpha$ and $\hat{\psi}_\beta$ converge to the actual values in a very short duration. It can be also seen that the estimated virtual flux could follow its actual value very well during steady state despite the variation of the active power. On the contrary, the prior virtual-flux observer-based FCS-MPC shown in Figure 7 (b) presents very large error between the estimated power and the actual power, due to relatively slow converging rate of the estimated virtual flux. Additionally, high inrush current can be seen for the prior virtual-flux observer-based FCS-MPC. The dynamic performance is improved because no filter is applied in the proposed method. On the contrary, the prior method usually employs low-pass filter or bandpass filter to solve the issue of dc-drift in the pure integral. The incorporation of the filter inevitably increase delay in the estimation [28]. From this comparative study, it is clear that the proposed SMVFO can safely start a PWM rectifier without grid voltage sensors.

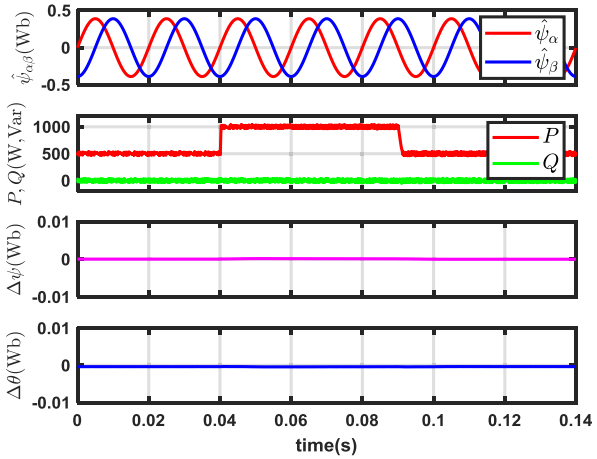

FIGURE 8. Simulated estimation errors of virtual flux during steady and dynamic process.

Figure 8 presents the estimation errors of the phase angle and the magnitude of the virtual flux to further reveal the performance of the proposed SMVFO. $\Delta\psi = |\boldsymbol{\psi}| - \left|\hat{\boldsymbol{\psi}}\right|$ is the estimation error of the magnitude and $\Delta\theta =$ angle $(\boldsymbol{\psi})$ −angle$(\hat{\boldsymbol{\psi}})$ is the error for the phase angle. These two errors both keep at zero during the whole process including steady and dynamic states, proving the virtual flux tracking ability of the proposed method.

A comparison of the current total harmonic distortion (THD) between the proposed SMVFO based FCS-MPC and the conventional measured grid voltage-based FCS-MPC is shown in Figure 9.

For the steady state, the proposed method could achieve the similar performance as the conventional sensor-based FCS-MPC with ideal measurement. Due to the filtering effect of the virtual flux, the current THD for SMVFO based FCS-MPC is slightly lower than the voltage sensor-based method.

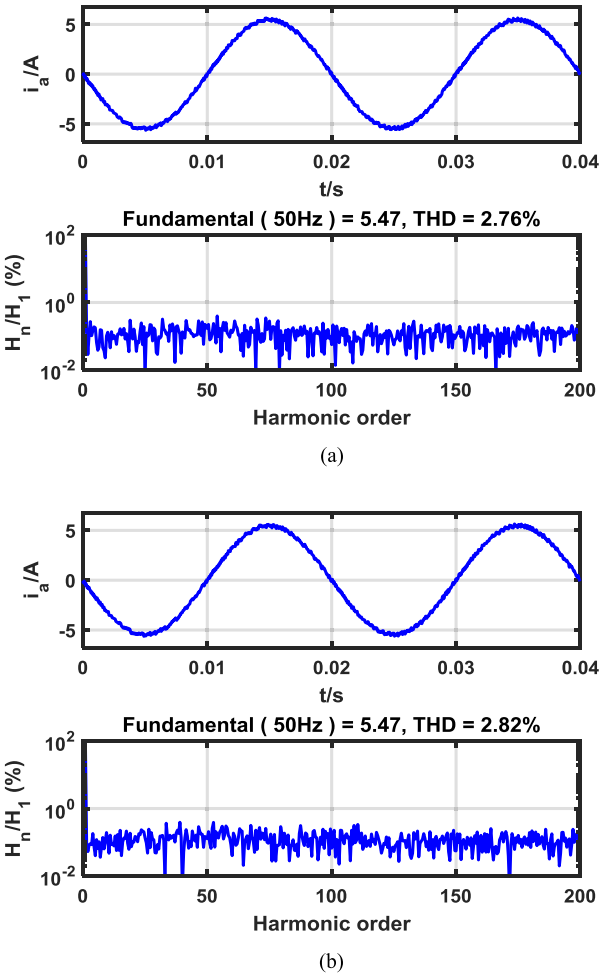

FIGURE 9. Comparisons of current THD. (a) FCS-MPC based on the proposed SMVFO. (b) Conventional FCS-MPC with measured grid voltage.

B. EXPERIMENTAL ANALYSIS

In order to further evaluate the proposed SMVFO based FCS-MPC method, a prototype of a two-level PWM rectifier is adopted to conduct corresponding experiments. The algorithm is implemented on a 32-bit floating point DSP TMS320F28335. Probes are directly adopted to acquire the actual grid voltage and current waveforms. An on-board DA converter is used for obtaining the internal variables. All the data of waveforms are acquired by a Yokogawa's DL850E scopecoder.

The startup performance of the proposed SMVFO based FCS-MPC and the prior virtual flux observer-based FCS-MPC are shown in Figure 10. The diode rectifier setup the DC-link voltage before the control system is energized. After the activation of the control system, the reference active power is 1000W. The fast converging ability of the grid voltage estimator of the proposed method ensure that no high inrush current occurs as shown in Figure 10 (a) and guarantee safe operation of the proposed method during startup process. By comparison, the prior virtual-flux observer-based FCS-MPC shows significant distortion during startup process

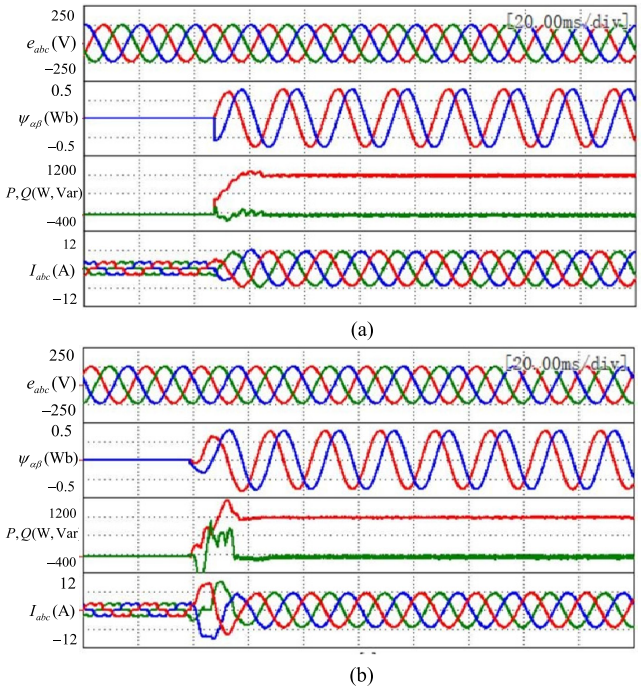

FIGURE 10. Experimental results of startup response. (a) SMVFO based FCS-MPC. (b) Prior virtual-flux observer based FCS-MPC.

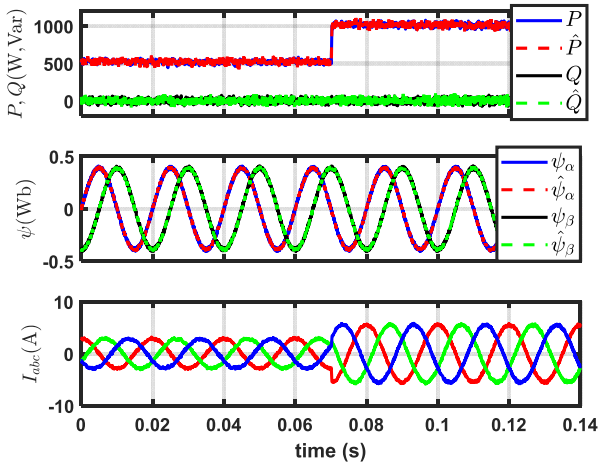

FIGURE 11. Dynamic responses for SMVFO based FCS-MPC.

in Figure 10 (b) because of slower converging speed. As a result, the peak current of the prior observer-based FCS-MPC is much larger than that in the proposed method. In conclusion, the PWM rectifier can be safely started by the developed SMVFO based FCS-MPC without voltage sensors.

The dynamic performance of the proposed method is shown in Figure 11 where the reference of active power changes from 500W to 1000W. Due to the limited channels of DA converter, the actual power P and Q are obtained by transferring the data of the measured grid voltage and grid current to the PC and then the waveform is plotted in Matlab. It can be seen that the estimated active power and reactive power are in accordance with that computed by measured grid voltage and current, which indirectly justify the accuracy of

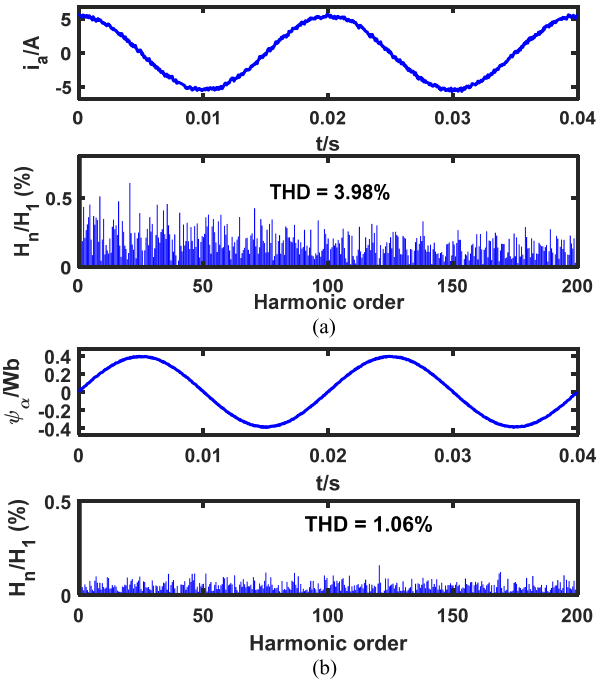

FIGURE 12. Spectrum analysis of (a) grid current and (b) the estimated virtual flux.

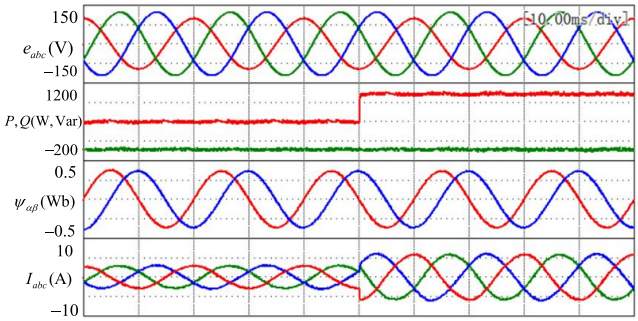

FIGURE 13. Performance of the proposed method with unbalanced grid voltages.

the estimated virtual flux. With the proposed SMVFO based FCS-MPC, the actual active power can track its reference quickly. Although P changes sharply, the estimated virtual flux could still follow the actual virtual flux well, indicating excellent robustness of the proposed SMVFO against external disturbances.

The THD comparisons of the estimated grid voltage and measured current are shown in Figure 12. With the proposed method, the shape of grid current is sinusoidal and the THD is 3.98% when the harmonic order is calculated up to 200th. Moreover, the estimated virtual flux is clean without significant ripples, indicating good filtering capacity of the proposed SMVFO against noises and harmonics.

In practical application, there might be imbalance in three-phase grid voltages [21]. Figure 13 shows dynamic responses of the proposed SMVFO based FCS-MPC when 20% voltage dip in phase-A is applied. The active power reference is suddenly stepped from 500 W to 1000W around 0.5s. It can

be seen that the proposed method works stably and well even under unbalanced grid conditions. The actual power can track its reference quickly during dynamic process. There are no obvious harmonics in the estimated virtual flux. However, three-phase grid currents are slightly distorted. To further improve the control performance, a proper power control scheme, such as [35], can be applied to compensate the impact of the unbalanced grid voltages, which will be investigated in future research.

VI. CONCLUSION

A SMVFO based FCS-MPC is proposed in this paper. The proposed method has the fast power control ability and at the same time doesn't require the grid voltage measurement. The estimated virtual flux can accurately track its actual value. The implementation of the whole control system is simple but the performance is not compromised. The simulation and experimental tests justify that the estimated virtual flux from the proposed SMVFO is coincident with the actual virtual flux while attenuating undesired harmonics.

Compared with the prior method, the proposed SMVFO exhibits better dynamic response. The obtained results validate that satisfactory steady-state performance and fast dynamic responses could be achieved by the SMVFO assisted FCS-MPC without grid voltage sensors.

REFERENCES

[1] L. Xie, H. Su, S. Lu, and L. Xie, "Linear mismatched model based offset-free MPC for nonlinear constrained systems with both stochastic and deterministic disturbances and its application to CSTR," *IEEE Access*, vol. 6, pp. 69172–69184, 2018.

[2] Y. Zhou and X. Tao, "Robust safety monitoring and synergistic operation planning between time- and energy-efficient movements of high-speed trains based on MPC," *IEEE Access*, vol. 6, pp. 17377–17390, 2018.

[3] E. Fuentes, C. A. Silva, and R. M. Kennel, "MPC implementation of a quasi-time-optimal speed control for a PMSM drive, with inner modulated-FS-MPC torque control," *IEEE Trans. Ind. Electron.*, vol. 63, no. 6, pp. 3897–3905, Jun. 2016.

[4] Q. Chen, X. Luo, L. Zhang, and S. Quan, "Model predictive control for three-phase four-leg grid-tied inverters," *IEEE Access*, vol. 5, pp. 2834–2841, 2017.

[5] A. A. Ahmed, B. K. Koh, and Y. Il Lee, "A comparison of finite control set and continuous control set model predictive control schemes for speed control of induction motors," *IEEE Trans. Ind. Informat.*, vol. 14, no. 4, pp. 1334–1346, Apr. 2018.

[6] M. Narimani, B. Wu, V. Yaramasu, and N. R. Zargari, "Finite control-set model predictive control (FCS-MPC) of nested neutral point-clamped (NNPC) converter," *IEEE Trans. Power Electron.*, vol. 30, no. 12, pp. 7262–7269, Dec. 2015.

[7] C. S. Lim, E. Levi, M. Jones, N. A. Rahim, and W. P. Hew, "FCS-MPC-based current control of a five-phase induction motor and its comparison with PI-PWM control," *IEEE Trans. Ind. Electron.*, vol. 61, no. 1, pp. 149–163, Jan. 2014.

[8] K. Shen, J. Feng, and J. Zhang, "Finite control set model predictive control with feedback correction for power converters," *CES Trans. Elect. Mach. Syst.*, vol. 2, no. 3, pp. 312–319, Sep. 2018.

[9] N. S. Hasan, N. Rosmin, D. A. A. Osman, and A. H. Musta'amal, "Reviews on multilevel converter and modulation techniques," *Renew. Sustain. Energy Rev.*, vol. 80, pp. 163–174, Dec. 2017.

[10] J. Falck, M. Andresen, and M. Liserre, "Thermal-based finite control set model predictive control for IGBT power electronic converters," in *Proc. IEEE Energy Convers. Congr. Expo. (ECCE)*, Sep. 2016, pp. 1–7.

[11] A. Lashab, D. Sera, J. M. Guerrero, L. Mathe, and A. Bouzid, "Discrete model-predictive-control-based maximum power point tracking for PV systems: Overview and evaluation," *IEEE Trans. Power Electron.*, vol. 33, no. 8, pp. 7273–7287, Aug. 2018.

[12] M. R. Nasiri, S. Farhangi, and J. Rodríguez, "Model predictive control of a multilevel CHB STATCOM in wind farm application using diophantine equations," *IEEE Trans. Ind. Electron.*, vol. 66, no. 2, pp. 1213–1223, Feb. 2019.

[13] N. Hoffmann, M. Andresen, F. W. Fuchs, L. Asiminoaei, and P. B. Thøgersen, "Variable sampling time finite control-set model predictive current control for voltage source inverters," in *Proc. IEEE Energy Convers. Congr. Expo. (ECCE)*, Sep. 2012, pp. 2215–2222.

[14] M. Siami, D. A. Khaburi, and J. Rodriguez, "Simplified finite control set-model predictive control for matrix converter-fed PMSM drives," *IEEE Trans. Power. Electron.*, vol. 33, no. 3, pp. 2438–2446, Mar. 2018.

[15] Y. B. Zbede, S. M. Gadoue, and D. J. Atkinson, "Model predictive MRAS estimator for sensorless induction motor drives," *IEEE Trans. Ind. Electron.*, vol. 63, no. 6, pp. 3511–3521, Jun. 2016.

[16] Z. Song, W. Chen, and C. Xia, "Predictive direct power control for three-phase grid-connected converters without sector information and voltage vector selection," *IEEE Trans. Power Electron.*, vol. 29, no. 10, pp. 5518–5531, Oct. 2014.

[17] Y. Son and J.-I. Ha, "Direct power control of a three-phase inverter for grid input current shaping of a single-phase diode rectifier with a small DC-link capacitor," *IEEE Trans. Power Electron.*, vol. 30, no. 7, pp. 3794–3803, Jul. 2015.

[18] S. Kwak and J. C. Park, "Model-predictive direct power control with vector preselection technique for highly efficient active rectifiers," *IEEE Trans Ind. Informat.*, vol. 11, no. 1, pp. 44–52, Feb. 2015.

[19] F. A. Ramírez, M. A. Arjona, and C. Hernández, "A novel parameter-independent fictive-axis approach for the voltage oriented control of single-phase inverters," *J. Power Electron.*, vol. 17, no. 2, pp. 533–541, 2017.

[20] M. Jamma, M. Barara, M. Akherraz, and B. A. Enache, "Voltage oriented control of three-phase PWM rectifier using space vector modulation and input output feedback linearization theory," in *Proc. 8th Int. Conf. Electron., Comput. Artif. Intell. (ECAI)*, Jun./Jul. 2016, pp. 1–8.

[21] Y. Cho and K.-B. Lee, "Virtual-flux-based predictive direct power control of three-phase PWM rectifiers with fast dynamic response," *IEEE Trans. Power Electron.*, vol. 31, no. 4, pp. 3348–3359, Apr. 2016.

[22] Y. K. Tao, Q. H. Wu, W. H. Tang, and L. Wang, "Voltage sensorless predictive direct power control for renewable energy integration under grid fault conditions," in *Proc. IEEE Innov. Smart Grid Technol.-Asia (ISGT ASIA)*, Nov. 2015, pp. 1–5.

[23] Y. A.-R. I. Mohamed and E. F. El-Saadany, "Adaptive discrete-time grid-voltage sensorless interfacing scheme for grid-connected DG-inverters based on neural-network identification and deadbeat current regulation," *IEEE Trans. Power Electron.*, vol. 23, no. 1, pp. 308–321, Jan. 2008.

[24] Y. A.-R. I. Mohamed, E. F. El-Saadany, and M. M. A. Salama, "Adaptive grid-voltage sensorless control scheme for inverter-based distributed generation," *IEEE Trans. Energy Convers.*, vol. 24, no. 3, pp. 683–694, Sep. 2009.

[25] M. Malinowski, M. P. Kazmierkowski, S. Hansen, F. Blaabjerg, and G. D. Marques, "Virtual-flux-based direct power control of three-phase PWM rectifiers," *IEEE Trans. Ind. Appl.*, vol. 37, no. 4, pp. 1019–1027, Jul. 2001.

[26] L. A. Serpa, S. D. Round, and J. W. Kolar, "A virtual-flux decoupling hysteresis current controller for mains connected inverter systems," *IEEE Trans. Power Electron.*, vol. 22, no. 5, pp. 1766–1777, Sep. 2007.

[27] P. Antoniewicz and M. P. Kazmierkowski, "Virtual-flux-based predictive direct power control of AC/DC converters with online inductance estimation," *IEEE Trans. Ind. Electron.*, vol. 55, no. 12, pp. 4381–4390, Dec. 2008.

[28] J. G. Norniella *et al.*, "Improving the dynamics of virtual-flux-based control of three-phase active rectifiers," *IEEE Trans. Ind. Electron.*, vol. 61, no. 1, pp. 177–187, Jan. 2014.

[29] L. Sheng, W. Li, Y. Wang, M. Fan, and X. Yang, "Sensorless control of a shearer short-range cutting interior permanent magnet synchronous motor based on a new sliding mode observer," *IEEE Access*, vol. 5, pp. 18439–18450, 2017.

[30] S. Chi, Z. Zhang, and L. Xu, "Sliding-mode sensorless control of direct-drive PM synchronous motors for washing machine applications," *IEEE Trans. Ind. Appl.*, vol. 45, no. 2, pp. 582–590, Mar. 2009.

[31] C. Edwards, S. K. Spurgeon, and R. J. Patton, "Sliding mode observers for fault detection and isolation," *Automatica*, vol. 36, no. 4, pp. 541–553, 2000.
[32] X. Xiao, Y. Zhang, X. Song, T. Yildirim, and F. Zhang, "Virtual flux direct power control for PWM rectifiers based on an adaptive sliding mode observer," *IEEE Trans. Ind. Appl.*, vol. 54, no. 5, pp. 5196–5205, Sep./Oct. 2018.
[33] J. D. Barros, J. F. A. Silva, and G. A. Jesus, "Fast-predictive optimal control of NPC multilevel converters," *IEEE Trans. Ind. Electron.*, vol. 60, no. 2, pp. 619–627, Feb. 2013.
[34] D. P. Marcetic, I. R. Krcmar, M. A. Gecic, and P. R. Matic, "Discrete rotor flux and speed estimators for high-speed shaft-sensorless IM drives," *IEEE Trans. Ind. Electron.*, vol. 61, no. 6, pp. 3099–3108, Jun. 2014.
[35] H. Yang, Y. Zhang, J. Liang, J. Liu, N. Zhang, and P. D. Walker, "Robust deadbeat predictive power control with a discrete-time disturbance observer for PWM rectifiers under unbalanced grid conditions," *IEEE Trans. Power Electron.*, vol. 34, no. 1, pp. 287–300, Jan. 2019.

JIEJUNYI LIANG received the B.S. degree in mechanical design, manufacturing, and automation from the Huazhong University of Science and Technology, Wuhan, China, in 2012, the M.S. degree in electromechanical engineering from the University of Macau, Macau, China, in 2015, and the Ph.D. degree in mechanical engineering from the Faculty of Engineering and Information Technology, University of Technology Sydney, in 2018. He is currently a Research Fellow with the School of Automotive Engineering, Wuhan University of Technology, China.

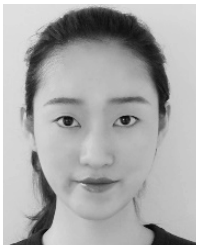

HAIQING WANG received the B.S. degree from Liaoning Shihua University, China, in 2015, and the M.S. degree in mechanical engineering from the Faculty of Engineering and Information Technology, University of Technology Sydney, in 2018, where she is currently a Research Assistant.

ZHENGFENG YAN received the B.Sc. degree in mechanical engineering from the University of Chongqing, in 1991, the M.Sc. degree in industry engineering from the Huazhong University of Science and Technology, in 2003, and the Ph.D. degree in mechanical manufacturing and automation from the Wuhan University of Technology, in 2009. Since 2011, he has been a Full Professor with the Hefei University of Technology. He has authored over 30 peer-review indexed journal papers, international conference papers, and book chapters. He has also been participating in over 10 research projects supported by the regional and national government and companies.